Journal Name

ARTICLE

Solvent-Induced Surface Hydroxylation of Layered Perovskite $Sr_3FeCoO_{7-\delta}$ for Enhanced Oxygen Evolution Catalysis

Kongliang Xu,[ab]‡ Fang Song,*[b]‡ Jun Gu,[b] Xiang Xu,[b] Zhenning Liu*[a,] and Xile Hu*[b]

Received 00th January 20xx,
Accepted 00th January 20xx

DOI: 10.1039/x0xx00000x

www.rsc.org/

Efficient oxygen evolution reaction (OER) catalysts made of earth abundant elements are essential for the cost-effective generation of solar fuels. Surface modification is a novel strategy to enhance the activity of OER catalysts, however, it is commonly done under harsh and energy intensive conditions. Herein, we present a facile approach of solvent treatment to hydroxylate the surface of a layered perovskite, $Sr_3FeCoO_{7-\delta}$. The catalytic activity correlates with the degree of surface hydroxylation, which influences the absorption energy of intermediates on the surface. The optimized catalyst exhibits activity higher than the current benchmark perovskite OER catalysts. The work introduces a mild and convenient method for surface modification, which may be applicable for the improvement of other nanoscale electrocatalysts.

1 Introduction

Oxygen evolution catalysts play a pivotal role in water-splitting devices.[1] Precious metal oxides, such as IrO_2 and RuO_2, are state-of-art oxygen evolution reaction (OER) catalysts, but their scarcity, high cost, and poor durability pose a significant limitation to large-scale practical applications.[2, 3] Hence, earth-abundant OER electrocatalysts are of great research interest.[4, 5] Perovskite oxides (ABO_3 type) have long been considered as a promising replacement of precious metal-based catalysts.[6-8]

Optimization of the absorption energy of the intermediates on active sites of perovskites is necessary to improve their activity.[8] A widely used approach is cation substitution (A or/and B sites).[9-12] This approach has led to the discovery of new perovskite OER catalysts and even descriptors (such as e_g filling and M-OH bond strength) that are useful for the prediction and design of efficient catalysts.[9-12] Another approach is to improve the activity without changing compositions. This has been achieved by phase tuning and introduction of oxygen vacancies. However, high-temperature annealing under sophisticated conditions are often required.[13-17] Ruddlesden-Popper (RP) type perovskite oxides (formula of $A_{n+1}B_nO_{3n+1}$) have periodic layered structures, which vary dependent on the n value. RP perovskites have been studied as OER catalysts, but their activity is still inferior to state-of-the-art catalyst.[18-21]

Herein, we show that solvent treatment can be applied to enhance the OER activity of a layered perovskite $Sr_3FeCoO_{7-\delta}$ (n=2). The best catalyst is obtained when treated by N-methyl-2-pyrrolidone (NMP), which exhibits an overpotential of 343±4.4 mV at 10 mA cm^{-2}, ranking among the most active perovskite OER catalysts to date. Solvent-induced surface hydroxylation is proposed to afford optimized absorption energy of OER intermediates (*OH, *O and *OOH) on the surface.

2 Experimental

2.1 Synthesis of layered perovskite $Sr_3FeCoO_{7-\delta}$

Layered perovskite $Sr_3FeCoO_{7-\delta}$ was synthesized using a liquid-based ethylenediaminetetraacetic acid (EDTA)-citrate complexing method according to the previous literatures.[22, 23] In details, stoichiometric amounts of $Sr(NO_3)_2$ (0.75 mM), $Co(NO_3)_2{\cdot}6H_2O$ (0.25 mM) and $Fe(NO_3)_3{\cdot}9H_2O$ (0.25 mM) were dissolved in distilled water (60 mL). EDTA (1.25 mM) and citric acid (2.5 mM) were then added as complexing agents in sequence at a mole ratio of 1:1:2 for total metal ions/EDTA/citric acid. The obtained transparent gel was evaporated in a hot-oil bath (120 °C) overnight to form a solid precursor, and the resultant dry gel was decarbonized in an electric furnace at 450 °C for 3-4 h. This intermediate product was grinded and calcined in air at 1000 °C for *ca.*110 h with three intermediate grindings.

2.2 Solvent treatment of layered perovskite $Sr_3FeCoO_{7-\delta}$

Five common solvents (*i.e.* isopropyl alcohol (IPA), formamide (FA), dimethylformamide (DMF), N-methyl-2-pyrrolidone (NMP), dimethyl sulfoxide (DMSO)) were used for the solvent treatment. In details, 5 mg perovskites of $Sr_3FeCoO_{7-\delta}$, 0.25 mL water (5 %) and 4.75 mL solvents (95 %) were added together and stirred for 7 days for the treatment. The role of the 5 %

[a] Key Laboratory of Bionic Engineering (Ministry of Education), College of Biological and Agricultural Engineering, Jilin University, Changchun, Jilin 130022, P. R. China. E-mail: liu_zhenning@jlu.edu.cn
[b] Laboratory of Inorganic Synthesis and Catalysis, Institute of Chemical Sciences and Engineering, École Polytechnique Fédérale de Lausanne (EPFL), EPFL-ISIC-LSCI, BCH 3305, Lausanne 1015 Switzerland. E-mail: sofa0318@gmail.com or xile.hu@epfl.ch. Web: http://lsci.epfl.ch

† Electronic Supplementary Information (ESI) available: Experimental details and supplementary figures. See DOI: 10.1039/x0xx00000x

‡ These authors contributed equally to this work

water is to ensure the full water intercalation in the $(SrO)_2$ double-layer block. The NMP treated layered perovskite $Sr_3FeCoO_{7-\delta}$ were collected by centrifugation (8000 rpm for 5 minutes) and washed with alcohol for 3 times for the structure and morphology characterization and electrochemical evaluation.

2.3 Material Characterization

XRD patterns were recorded on an X'Pert Philips diffractometer with monochromatic CuKa radiation (λ=1.540598 Å) and a fast Si-PIN multi-strip detector. For the solid powder, the perovskites were dried and grinded (destroy the preferred orientation), and pressed on the glass substrate to form a plane for XRD characterization. For suspension cast film, the perovskites with alcohol were directly dried on glass substrate at room temperature and then used for XRD characterization. SEM images were examined by a Phillips (FEI) XLF-30 FEG SEM. TEM was examined by a FEI Tecnai Osiris TEM equipped with high-brightness field emission gun (XFEG). Samples for TEM were prepared by drop-drying the samples from their diluted ethanol suspensions onto carbon-coated copper grids. Energy-dispersive X-ray spectroscopy (EDX) patterns and mapping images were taken on the FEI Tecnai Osiris TEM under a scanning TEM modal. The elemental ratio was calculated from the Kα peak area of each element, using the software of ESPRIT 2 (Bruker). XPS measurements were performed on a PHI5000 Versa Probe II XPS system by Physical Electronics (PHI) with a detection limit of one atomic percent. Monochromatic X-rays were generated by an Al Kα source (14,867 eV). The diameter of the analyzed area is 10 µm. TGA characterizations were performed on a TGA 4000 from Perkin Elmer. The ramping rate of temperature was 10 °C·min^{-1}.

2.4 Electrode preparation

Glassy carbon electrodes with a diameter of 3 mm were used. They were polished with alpha alumina powder (0.3 micron from CH instruments) suspended in deionized water on a Nylon polishing pad (CH instruments) and with gamma alumina powder (0.05 micron from CH instruments) suspended in distilled water on a micro-cloth polishing pad (CH instruments). After each polish, the electrodes were thoroughly rinsed with deionized water and cleaned in acetone by sonication for ~10 s. Catalysts (5 mg) and carbon nanotubes (CNT, 1 mg) were dispersed in mixed solvent of deionized water (1 mL) and 2-propanol (0.25 mL) via sonication for more than 0.5 h. 10 µL Nafion solution (5 wt%) was added into the corresponding suspension to increase the binding strength. Suspensions were then drop-casted on a glassy carbon electrode (5 µL suspensions) by micropipette (variable volume: 1-10 µL), and the solvent was allowed to be evaporated at 70 °C for around 10 minutes. The catalyst loadings were 0.283 mg cm^{-2}.

2.5 Electrochemical tests

Electrochemical characterizations including cyclic voltammetry (CV), linear sweep voltammetry (LSV) and chronopotentiometry were carried out on a Gamry Reference 3000 electrochemical instrument using a three-electrode electrochemical system. A 1M KOH solution was used as electrolyte, and an Ag/AgCl electrode with saturated KCl filling solution and Pt wire were used as reference and counter electrodes, respectively. Before test, the reference electrode was measured against another unused Ag/AgCl reference electrode stored in saturated KCl solution. Calibration of Ag/AgCl reference electrodes was done by measuring the reversible hydrogen electrode (RHE) potential using a Pt electrode under a H_2 atmosphere. During the test, Ag/AgCl reference electrode was constructed to a double-junction electrode to minimize contact between KOH and KCl. CVs were performed at a scan rate of 5 mVs^{-1}, and the average of the two potentials at which the current crossed zero was taken to be the thermodynamic potential for the hydrogen electrode reaction. In 1M KOH electrolytes, E vs. RHE = $E_{vs.\ Ag/AgCl}$ + 1.009 V, and overpotential (η) for OER was $\eta = E_{vs.\ RHE}$ -1.23 V = $E_{vs.\ Ag/AgCl}$ - 0.221 V. Ohmic drop correction was performed using the current interrupt method by the potentiostat. Cyclic voltammograms (CVs) were performed between 0.2 and 0.6 V vs. Ag/AgCl in 1M KOH at a scan rate of 20 mV s^{-1}. LSV was applied to record the catalytic activity from 0.2 to 0.55-0.6 V vs. Ag/AgCl at a scan rate of 5 mV s^{-1}. AC impedance measurements were taken on charged catalysts at 0.5 V versus Ag/AgCl.[24] The frequency range is from 100 MHz to 0.1 Hz. The double-layer capacitance values (C_{dl}) were obtained through fitting of the impedance spectrum using an equivalent circuit (Randles circuit). The electrochemically active surface area (ECSA) was calculated from the double-layer capacitance according to equation: ECSA = C_{dl}/C_s, where the C_s is the specific capacitance. The C_s is around 80 µF cm^{-2} for metal oxides. The roughness factor (RF) was calculated by dividing the estimated ECSA by the geometric area of the electrode. Specific current density J_s was calculated according to equation: $J_s = J/RF$, where J is the geometric current density.

3 Results and discussion

Layered perovskite $Sr_3FeCoO_{7-\delta}$ was synthesized by a liquid-based complexing method with ethylenediaminetetraacetic acid (EDTA) and citrate, followed by medium temperature decarbonation (450 °C for 3-4 h) and high temperature annealing (1000 °C for *ca.*110 h) in air.[22, 23] The obtained product was black in color and was grinded before solvent treatment. As shown in the scanning electron microscopy (SEM) images (**Fig. 1**a and Fig. S1, ESI†), the perovskites are several micrometers in dimension similar to common perovskites synthesized via high temperature annealing.[9, 11] The micron-sized aggregates were made of several smaller particles (Fig. S2, ESI†). Sr, Fe, and Co are homogeneously dispersed in the particles as revealed by elemental mapping (Fig. 1b), with the ratio of Sr:Fe:Co as 3.2:1.1:1 (Fig. S3, ESI†).

The layered perovskite is of high crystallinity, as revealed by the sharp diffraction peaks of X-ray diffraction (XRD) pattern (Fig. 1c), which agrees with the standard profile of water-

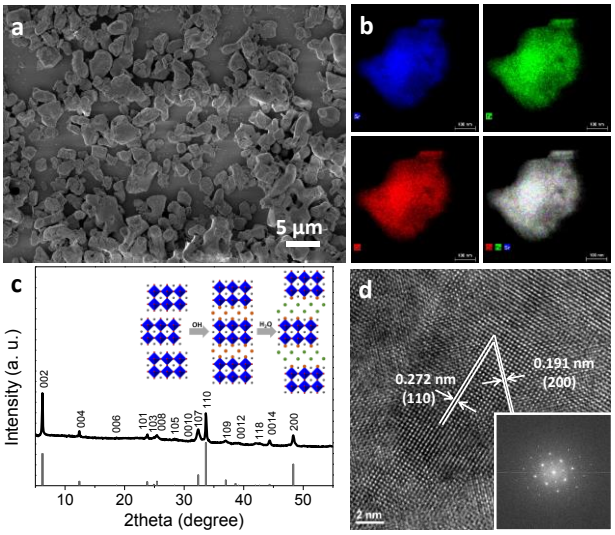

Fig. 1 Structure characterization of hydroxylated layered perovskite of $Sr_3FeCoO_{7-\delta}$. (a) SEM image; (b) Elemental mapping images: blue for Sr, green for Fe and red for Co; (c) XRD pattern with inset showing the structure evolution induced by the hydroxylation and hydration (oxygen vacancies are not shown for clear illustration); Standard XRD pattern of hydrated Sr_3MO_7 is plotted using data in ref. 25;[25] (d) HR-TEM image and the corresponding FFT pattern (inset).

derivative Ruddlesden-Popper type layered structure (I4/mmm, a=3.82 Å, c=28.03 Å).[22, 25] The strong diffraction peaks of (00n) (n=2, 4, 6, 8, 10, 12 and 14) planes correspond to a large interlayer space of 2.8 nm, suggesting the hydroxylation and hydration of layered perovskite $Sr_3FeCoO_{7-\delta}$.[25, 26] The structure evolution induced by the hydroxylation and hydration is shown in the inset of Fig. 1c. Although both hydroxylation and hydration exist, the sample is called hydroxylated layered perovskites for simplicity. Lattice fringes on the high-resolution transmission electron microscopy (HR-TEM) image have revealed the plane spacings of 0.272 nm and 0.191 nm (Fig. 1d), which can be indexed to the planes of (110) and (200) based on the corresponding FFT image (inset of Fig. 1d).[22, 27]

Liquid exfoliation method was adopted in an attempt to delaminate the micro-sized powder to 2D nano-flakes, given the large interlayer space observed for the obtained layered perovskite $Sr_3FeCoO_{7-\delta}$ and the capability of water interaction.[28, 29] To our surprise, although the delamination was unsuccessful (Fig. S4, ESI†), the catalytic activities of the catalysts treated with different solvents in presence of 5 vol% H_2O have been significantly enhanced for oxygen evolution catalysis. The OER catalysis was tested in a three-electrode system with 1 M KOH as the electrolyte.[30, 31] Typical polarization curves are shown in **Fig. 2**a for hydroxylated layered perovskites before and after 7-day treatment with N-methyl-2-pyrrolidone (NMP). Linear sweep voltammetry (LSV) scan shifted towards lower potential after the solvent treatment, indicating that lower overpotential was required to reach the same current density (J) for the solvent-treated sample. It is noteworthy that the NMP-treated sample showed catalytic activity approaching that of nanoparticulated IrO_2. The overpotential (η) required to yield 10 mA cm^{-2} (η@10 mA cm^{-2}) is chosen as a standard parameter to evaluate the catalytic activity, as 10 mA cm^{-2} represents the current density from a device with 12% solar to hydrogen efficiency, which is at the upper end of a realistic device.[32] In total, five solvents (*i.e.* isopropyl alcohol (IPA), formamide (FA), dimethylformamide (DMF), dimethyl sulfoxide (DMSO), NMP) were used to treat the layered perovskites. The resultant η@10 mA cm^{-2} is shown in Fig. 2b for the as-obtained samples. All five solvent treatments resulted in some improvement of catalytic activity, which follows an order of NMP > DMF > DMSO > FA > IPA > untreated. For the most active sample (*i.e.* NMP-treated one), the η@10mA cm^{-2} is only 343±4.4 mV, which is 83 mV lower than the untreated layered perovskites. Moreover, the current density at η = 340 mV is 9.85 mA cm^{-2}, around 7.6 times higher than the untreated one (1.29 mA cm^{-2}). Considering the large particle size, it is not surprising that the catalytic activity of the perovskite catalysts is still inferior to that of metal oxide nanoparticles or carbon based OER catalysts with extremely high surface area.[33-36] On the other hand, the NMP-treated catalyst is comparable and even more active than the most active perovskites known to date (Table S1, ESI†),[9, 11, 17, 21, 23, 37, 38]. Increasing the surface area by reducing the particle size of this perovskite catalyst might improve further its activity.

By plotting overpotential against log (J), the kinetic parameters of OER by the two samples were calculated (Fig. 2c). The NMP treated perovskite $Sr_3FeCoO_{7-\delta}$ has a Tafel slope around 63 mV dec^{-1}, smaller than the untreated one (77 mV dec^{-1}). The lower Tafel slope indicates favorable kinetics for the NMP treated sample. The stability of the NMP treated sample was characterized by chronopotentiometric measurement, which exhibited relatively stable overpotential around 340 mV during 12-hour electrolysis at a constant current density of 10 mA cm^{-2} (Fig. 2d). By contrast, the nanoparticulated IrO_2 was much less durable. The overpotential for 10 mA cm^{-2} increased more than 30 mV in 10 h of electrolysis. The (HR-)TEM, EDX mapping and XPS analysis showed that the microstructure and composition of

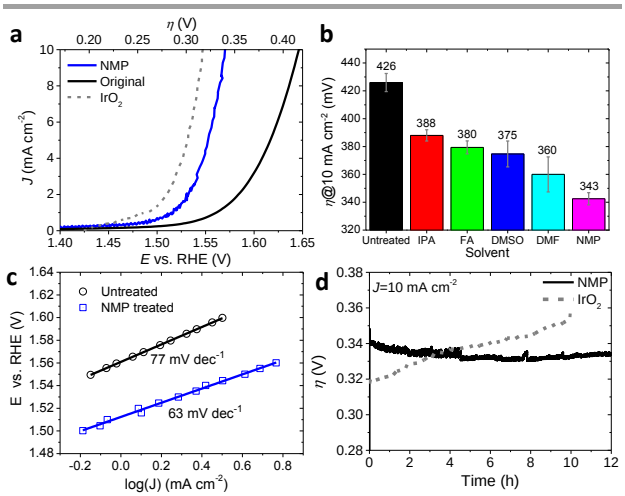

Fig. 2 Electrochemical characterization of hydroxylated layered perovskite of $Sr_3FeCoO_{7-\delta}$. (a) Polarization curves of untreated and NMP-treated perovskites and IrO_2 nanoparticles; (b) η@10mA cm^{-2} for perovskites after five treatments of different solvents; (c) Tafel plotting for perovskites before and after NMP-treatment; (d) Chronopotentiometric measurement of NMP-treated sample and IrO_2 nanoparticles at J = 10 mA cm^{-2} for 12 and 10 hours, respectively.

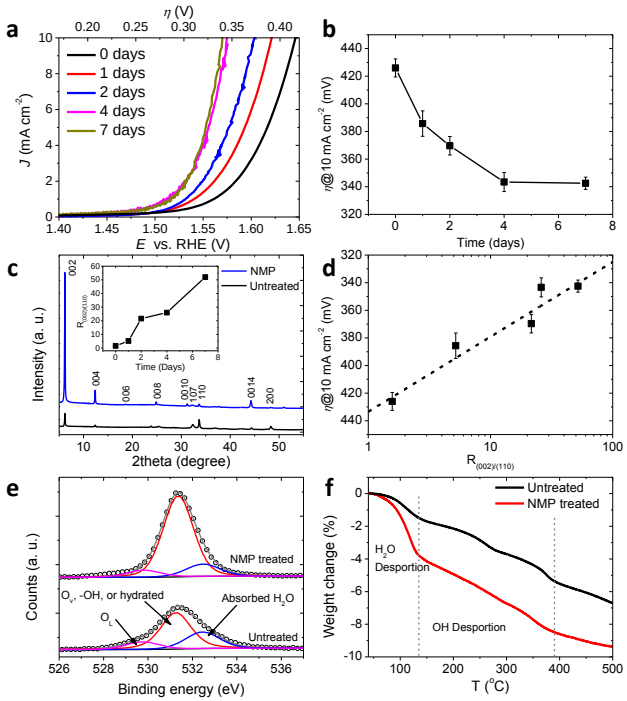

Fig. 3 Characterization of hydroxylated layered perovskite of $Sr_3FeCoO_{7-\delta}$ after NMP treatments of different durations. (a) Polarization curves; (b) η @10mA cm^{-2} plotted against different treatment durations; (c) XRD patterns of untreated and NMP-treated perovskites (7-day). Inset shows the $R_{002/110}$ ratios of different treatment durations; (d) η@10 mA cm^{-2} plotted against $R_{002/110}$; (e) High resolution XPS spectra for O_{1s}; (f) Thermogravimetric analysis of untreated and NMP-treated perovskites.

transition metal were retained for the perovskite catalyst after OER catalysis (Fig. S5 and Fig. S6, ESI†).

To understand the mechanism for the enhanced catalytic activity, the catalytic activity of NMP-treated perovskites were tracked by treatment duration. The polarization curves shifted towards lower potential with longer time of treatment (**Fig. 3**a). The resultant η@10 mA cm^{-2} is shown in Fig. 3b, which reveals that the OER catalytic activity becomes stable in 4 days. Yet, SEM and TEM images revealed no obvious difference in size and morphology for the treated and untreated samples (Fig. S7 and Fig. S8, ESI†). Although the BET surface area (Fig. S9, ESI†) has increased by 30% and the electrochemical active surface area increased by 150% (Table S2 and Fig. S10, ESI†) after the NMP treatment, such an increase is unlikely to fully account for the large improvement (7.6-fold) observed for the catalytic activity. Interestingly, it is found from XRD patterns that the peak corresponding to the (002) plane has elevated sharply with increasing treatment time (Fig. 3c). The relative intensity of (002) and (110) (denoted as $R_{002/110}$) increased from 1.6 to 52 in 7 days of NMP treatment (inset in Fig. 3c). Such large change has been reported in layered perovskite oxides before, and it was ascribed to the increasing degree of hydroxylation.[25] The augmented surface hydroxylation was first evidenced by the X-ray photoelectron spectroscopy (XPS) analysis. In the XPS spectra for O_{1s}, a significant peak corresponding to oxygen vacancies, hydroxyl groups or hydrated surface is present in both samples before and after solvent treatment (Fig. 3e). The

Table 1 Comparison of three layered perovskites on water content, $R_{002/110}$ and catalytic activity.

Layered perovskites	Water content (wt%)	OH content (wt%)	$R_{002/110}$	Overpotential (mV)	Tafel slope (mV dec^{-1})
Untreated	1.5	3.9	1.6	426±6.5	76.9
NMP-treated	3.8	4.7	26	343±4.4	62.6
Vacuum dried NMP-treated	0.25[a]	1.7[a]	0.74[b]	419±3.7[b]	77.5[b]

Note: [a] After vacuum drying, the sample was transferred to TGA measurement without inert gas protection. The small amount of water and OH are probably due to the hydroxylation and hydration during the transfer (air exposure). [b] XRD and OER catalytic activity were measured after the sample were exposed to air water for 3 days.

relative area of this peak increased by 8.7% after solvent treatment, which is consistent with the production of additional hydroxyl groups. The hydroxylation and hydration was further confirmed by the thermogravimetric analysis (TGA) in N_2 atmosphere (Fig. 3f and **Table 1**). The weight loss before 135 °C can be attributed to the loss of absorbed water, and the loss between 135 °C and 390 °C should result from the loss of hydroxyl groups (-OH).[19, 25, 26, 39] In comparison with the untreated one, more water (2.5-fold) and hydroxyl groups (1.2-fold) were lost from the NMP treated sample. Based on these results, it appears that the improved catalytic activity should relate to the surface hydroxylation that was induced by the solvent treatment.

To confirm the above hypothesis, the NMP-treated sample was dried in vacuum at 200 °C for 1 day and re-tested in TGA, XRD and OER catalysis. (Fig. S11, Fig. S12 and Fig. S13, ESI†) The water and hydroxyl contents of the obtained sample decreased to a level lower than the untreated sample (Table 1). Accordingly, the η@10mA cm^{-2} of the dehydroxylated sample (vacuum dried NMP-treated) increased from 343 mV to 419 mV (Table 1 and Fig. S13, ESI†). The decreased activity for the dehydroxylated sample gives another evidence that the activity improvement of the NMP-treated sample is due to hydroxylation and hydration induced by solvent treatment. It is noted that along with dehydroxylation, the XRD peak ratio of $R_{002/110}$ decreased to only 0.74. This suggests using $R_{002/110}$ as a semi-quantitative index to evaluate the degree of hydroxylation for RP-perovskites oxides (more discussion in Fig. S14 and Fig. S15, ESI†). By plotting the catalytic activities (η@10 mA cm^{-2}) against the log($R_{002/110}$), a linear correlation was revealed (Fig. 3d), providing a linkage between the catalytic activity and the degree of surface hydroxylation: the more surface hydroxylation, the larger $R_{002/110}$ and lower over-potential.

A hydroxylation-based mechanism has been proposed to explain the improved catalytic activity and rationalize the correlation between the catalytic activity and the degree of surface hydroxylation. **Fig. 4**a shows the hydroxylation process on the surface of layered perovskites. The presence of oxygen vacancies makes the hydroxylation thermodynamically feasible on the metal atoms nearby, while the speed and degree depend on the quantity of oxygen vacancies and the exposed environment.[25, 26, 39] Once layered perovskites are exposed to atmosphere or solvent containing water, surface water molecules dissociate into hydroxyl groups on the metal sites (M-O + Sr + H_2O → M-OH + Sr-OH, M is Co or Fe site), followed by

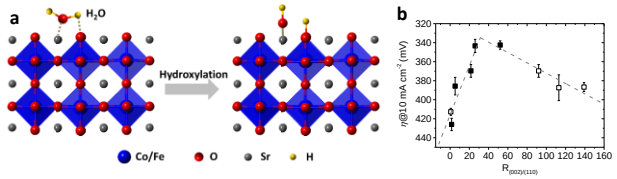

Fig. 4 (a) Surface hydroxylation of layered perovskite of $Sr_3FeCoO_{7-\delta}$ (oxygen vacancies are not shown for clear illustration) and (b) Volcano shape plotting of η@10 mA cm^{-2} against $R_{002/110}$.

subsequent intercalation of more water molecules (inset in Fig. 1c and Fig. 4a).[25, 26, 39] The number of Sr-OH is therefore linearly correlated to the degree of surface hydroxylation. The different degree of surface hydroxylation might be ascribed to the different polarity of solvents (see details in Fig. S16, ESI†). As shown in Fig. 4a, the formation of Sr-OH likely modifies the chemical environment of the intermediates (such as *OH, *O and *OOH) binding on M (Co/Fe) sites nearby (Fig. 4a), which allows the tuning of absorption energy. The absorption energies vary with the number of Sr-OH around (maximum 4 around each M site on the surface), which explains why the absorption energy of intermediates is correlated with the degree of hydroxylation in our case. Hydroxylation-dependent absorption energy has been reported by Shao-Horn et al. for ABO_3 type perovskites, where high affinity of oxides surface toward hydroxylation coincides with strong adsorption energies calculated for hydroxyl groups.[40] Accordingly, we propose that solvent treatment can tune the absorption energy of OER intermediates (such as *OH, *O and *OOH) on the surface by changing surface hydroxylation. According to the Sabatier principle, the catalytic activity will be maximized at an optimal, 'not too strong and not too weak', absorption energy.[41] Following this principle, the catalytic activity is likely to decrease when the degree of hydroxylation is too high for the layered perovskites presented here. To confirm this, a sample with a higher content of oxygen vacancies was synthesized and subjected to the solvent treatment. Higher degrees of surface hydroxylation were obtained in a shorter time. [25, 26, 39] As anticipated, the catalytic activity decreased when the $R_{002/110}$ > 52, and a 'volcano-like' plot was obtained (Fig. 4b).

4 Conclusions

In summary, we report that hydroxylated layered perovskites of $Sr_3FeCoO_{7-\delta}$ is a highly active and durable OER catalyst in alkaline conditions, with an overpotential of only 343±4.4 mV at 10 mA cm^{-2}. The high catalytic activity is ascribed to the increased surface hydroxylation induced by the solvent treatment. It is proposed that the surface hydroxylation modified the chemical environment of the active metal sites, and therefore allowed the optimization of the absorption energy of OER intermediates (*OH, *O and *OOH) on the surface. The strategy reported herein might also be applicable in improving the OER catalysts of other oxide catalysts with oxygen vacancies.

Conflicts of interest

There are no conflicts to declare.

Acknowledgements

This work is supported by the European Research Council (ERC) under the European Union's Horizon 2020 research and innovation programme (grant agreement n° 681292), the GazNat S.A., the Swiss Government Excellence Postdoc Fellowship Province Joint Fund (SXGJSF2017-2-4 and SXGJQY2017-1), JLUSTIRT Program of Jilin University and the China Scholarship Council. We thank Dr. Weiyan Ni (EPFL) and for help with XRD, the Interdisciplinary Center for Electron Microscopy at EPFL assistance in electron microscopic measurements and XPS, and Bila José Luis (EPFL) for the N_2 adsorption-desorption measurement.

Notes and references

1 N. S. Lewis and D. G. Nocera, *Proc. Natl. Acad. Sci.*, 2006, **103**, 15729-15735.
2 D. Galizzioli, F. Tantardini and S. Trasatti, *J. Appl. Electrochem.*, 1974, **4**, 57-67.
3 Y. Lee, J. Suntivich, K. J. May, E. E. Perry and Y. Shao-Horn, *J. Phys. Chem. Lett.*, 2012, **3**, 399-404.
4 Y. Jiao, Y. Zheng, M. Jaroniec and S. Z. Qiao, *Chem. Soc. Rev.*, 2015, **44**, 2060-2086.
5 N. T. Suen, S. F. Hung, Q. Quan, N. Zhang, Y. J. Xu and H. M. Chen, *Chem. Soc. Rev.*, 2017, **46**, 337-365.
6 J. O. Bockris and T. Otagawa, *J. Electrochem. Soc.*, 1984, **131**, 290-302.
7 D. Chen, C. Chen, Z. M. Baiyee, Z. Shao and F. Ciucci, *Chem. Rev.*, 2015, **115**, 9869-9921.
8 J. Hwang, R. R. Rao, L. Giordano, Y. Katayama, Y. Yu and Y. Shao-Horn, *Science*, 2017, **358**, 751-756.
9 J. Suntivich, K. J. May, H. A. Gasteiger, J. B. Goodenough and Y. Shao-Horn, *Science*, 2011, **334**, 1383.
10 A. Grimaud, K. J. May, C. E. Carlton, Y. L. Lee, M. Risch, W. T. Hong, J. G. Zhou and Y. Shao-Horn, *Nat. Commun.*, 2013, **4**, 2439.
11 Y. Zhu, W. Zhou, Z.-G. Chen, Y. Chen, C. Su, M. O. Tadé and Z. Shao, *Angew. Chem. Int. Ed.*, 2015, **54**, 3897-3901.
12 J. T. Mefford, X. Rong, A. M. Abakumov, W. G. Hardin, S. Dai, A. M. Kolpak, K. P. Johnston and K. J. Stevenson, *Nat. Commun.*, 2016, **7**, 11053.
13 N.-L. Wu, W.-R. Liu and S.-J. Su, *Electrochim. Acta*, 2003, **48**, 1567-1571.
14 S. Malkhandi, B. Yang, A. K. Manohar, A. Manivannan, G. K. S. Prakash and S. R. Narayanan, *J. Phys. Chem. Lett.*, 2012, **3**, 967-972.
15 J. Du, T. Zhang, F. Cheng, W. Chu, Z. Wu and J. Chen, *Inorg. Chem.*, 2014, **53**, 9106-9114.
16 J. Kim, X. Yin, K.-C. Tsao, S. Fang and H. Yang, *J. Am. Chem. Soc.*, 2014, **136**, 14646-14649.
17 K. Zhu, T. Wu, M. Li, R. Lu, X. Zhu and W. Yang, *J. Mater. Chem. A*, 2017, **5**, 19836-19845.
18 S. Choi, S. Yoo, J.-Y. Shin and G. Kim, *J. Electrochem. Soc.*, 2011, **158**, B995-B999.
19 T. Takeguchi, T. Yamanaka, H. Takahashi, H. Watanabe, T. Kuroki, H. Nakanishi, Y. Orikasa, Y. Uchimoto, H. Takano, N. Ohguri, M.

Matsuda, T. Murota, K. Uosaki and W. Ueda, *J. Am. Chem. Soc.*, 2013, **135**, 11125-11130.
20 R. C. Liu, F. L. Liang, W. Zhou, Y. S. Yang and Z. H. Zhu, *Nano Energy*, 2015, **12**, 115-122.
21 S. Liu, H. Luo, Y. Li, Q. Liu and J.-L. Luo, *Nano Energy*, 2017, **40**, 115-121.
22 M. Matvejeff, M. Lehtimäki, A. Hirasa, Y. H. Huang, H. Yamauchi and M. Karppinen, *Chem. Mater.*, 2005, **17**, 2775-2779.
23 Y. L. Zhu, W. Zhou, J. Yu, Y. B. Chen, M. L. Liu and Z. P. Shao, *Chem. Mater.*, 2016, **28**, 1691-1697.
24 A. S. Batchellor and S. W. Boettcher, *ACS Catal.*, 2015, **5**, 6680-6689.
25 D. Pelloquin, N. Barrier, D. Flahaut, V. Caignaert and A. Maignan, *Chem. Mater.*, 2005, **17**, 773-780.
26 D. Pelloquin, N. Barrier, A. Maignan and V. Caignaert, *Solid State Sci.*, 2005, **7**, 853-860.
27 Y. Bréard, C. Michel, M. Hervieu, F. Studer, A. Maignan and B. B. Raveau, *Chem. Mater.*, 2002, **14**, 3128-3135.
28 J. N. Coleman, M. Lotya, A. O'Neill, S. D. Bergin, P. J. King, U. Khan, K. Young, A. Gaucher, S. De, R. J. Smith, I. V. Shvets, S. K. Arora, G. Stanton, H. Y. Kim, K. Lee, G. T. Kim, G. S. Duesberg, T. Hallam, J. J. Boland, J. J. Wang, J. F. Donegan, J. C. Grunlan, G. Moriarty, A. Shmeliov, R. J. Nicholls, J. M. Perkins, E. M. Grieveson, K. Theuwissen, D. W. McComb, P. D. Nellist and V. Nicolosi, *Science*, 2011, **331**, 568-571.
29 V. Nicolosi, M. Chhowalla, M. G. Kanatzidis, M. S. Strano and J. N. Coleman, *Science*, 2013, **340**, 1226419.
30 F. Song, K. Schenk and X. L. Hu, *Energ. Environ. Sci.*, 2016, **9**, 473-477.
31 X. Xu, F. Song and X. L. Hu, *Nat. Commun.*, 2016, **7**, 12324.
32 F. Song and X. L. Hu, *Nat. Commun.*, 2014, **5**, 4477.
33 J. Lv, S. C. Abbas, Y. Huang, Q. Liu, M. Wu, Y. Wang and L. Dai, *Nano Energy*, 2018, **43**, 130-137.
34 C. Zhang, B. Wang, X. Shen, J. Liu, X. Kong, S. S. C. Chuang, D. Yang, A. Dong and Z. Peng, *Nano Energy*, 2016, **30**, 503-510.
35 X. Kong, K. Xu, C. Zhang, J. Dai, S. Norooz Oliaee, L. Li, X. Zeng, C. Wu and Z. Peng, *ACS Catal.*, 2016, **6**, 1487-1492.
36 K. Liu, C. Zhang, Y. Sun, G. Zhang, X. Shen, F. Zou, H. Zhang, Z. Wu, E. C. Wegener, C. J. Taubert, J. T. Miller, Z. Peng and Y. Zhu, *ACS Nano*, 2018, **12**, 158-167.
37 S. Yagi, I. Yamada, H. Tsukasaki, A. Seno, M. Murakami, H. Fujii, H. Chen, N. Umezawa, H. Abe, N. Nishiyama and S. Mori, *Nat. Commun.*, 2015, **6**, 8249.
38 B. Q. Li, C. Tang, H. F. Wang, X. L. Zhu and Q. Zhang, *Sci. Adv.*, 2016, **2**, e1600495.
39 L. Jantsky, H. Okamoto, A. Demont and H. Fjellvåg, *Inorg. Chem.*, 2012, **51**, 9181-9191.
40 K. A. Stoerzinger, W. T. Hong, G. Azimi, L. Giordano, Y.-L. Lee, E. J. Crumlin, M. D. Biegalski, H. Bluhm, K. K. Varanasi and Y. Shao-Horn, *J. Phys. Chem. C*, 2015, **119**, 18504-18512.
41 I. C. Man, H. Y. Su, F. Calle-Vallejo, H. A. Hansen, J. I. Martinez, N. G. Inoglu, J. Kitchin, T. F. Jaramillo, J. K. Norskov and J. Rossmeisl, *Chemcatchem*, 2011, **3**, 1159-1165.